On fracture toughness J_{IC} testing of martensitic stainless steels

Jianqiang Chen[1,*], Yves Verreman[1], Jacques Lanteigne[2]

[1]École Polytechnique de Montréal, C.P.6079, succ. Centre-ville, Montréal (Québec), Canada H3C 3A7

[2]Hydro-Québec, Institut de Recherche, 1800, boul. Lionel-Boulet, Varennes (Québec), Canada, J3X 1S1

* Corresponding author: jianqiang.chen@polymtl.ca

Abstract The objective of this research is to determine the best conditions to measure the fracture toughness of an ASTM A-743 grade CA-6NM stainless steel used in hydraulic turbine runners. The tests are performed on 12.7 mm and 25.4 mm thick compact tension (CT) specimens. Experimental results show that only the thicker specimen gives a valid test according to ASTM E1820 standard. However, very close crack initiation J_{IC} values are obtained with thinner specimens provided they are side-grooved. Thickness effect is exhibited both on the resistance curve *J-Δa* and the crack front during the stable crack propagation.
This paper is documented with both macroscopic and microscopic descriptions of fracture surfaces in the stable crack extension region.

Keywords J_{IC} fracture toughness, CA-6NM steel, CT specimen, thickness constraint effect

1. Introduction

The use of high-strength martensitic stainless steels in hydraulic turbine runners allows reduction in weight and cost of some components such as rotors, pumps and compressors. Designers take advantage of the high strength of these steels, which are also very little sensitive to corrosion and to cavitation damage [1-3]. Conventional turbine runners design is based on a so-called static stress design approach, which limits the Von Mises stress at operating condition to a prescribed fraction of the material yield stress (eg. $\sigma_e < 1/3\ \sigma_{YS}$). However, this approach does not guarantee reliability of runners as many other variables other than static stress can cause failure [4-5]. Welding blades, crown and band together unavoidably involves the presence of weld defects. It is not possible to detect accurately or size all defects with non-destructive inspection during the turbine runners manufacturing process, and due to economic reasons they cannot all repaired. Moreover, some defects can possibly be tolerated based on Fracture Mechanics assumptions for the whole runner lifetime (70 years). Hence, to determine a maximum allowable defect size, accurate knowledge of material properties and in particular fracture toughness need to be evaluated.

Measurement of fracture toughness K_{IC} is based on Linear-Elastic Fracture Mechanics (LEFM) [6-7]. It has been extensively used for high-strength and relatively brittle materials such as metals used in the aerospace industry and ceramics. However, the low carbon martensitic stainless steels used in hydraulic turbine runners manufacturing are in the range of immediate-strength and high toughness engineering materials. In order to get a valid K_{IC} test under small-scale yielding and plane-strain conditions, the required specimen can be as big as 300 mm in thickness for a compact tension specimen which is difficult to be tested in a common laboratory. Moreover, it is also impossible to fabricate steel in such dimension with homogeneous metallurgical properties (microstructure and texture) through the whole thickness. In this case, an alternative J_{IC} test method based on Elastic-Plastic Fracture Mechanics (EPFM) can be used [8-9]. J_{IC} test can be performed on a relatively small laboratory specimen. This testing method, firstly developed for the engineering materials used in nuclear power plants, is based on Rice's *J*-integral concept [10].

The objective of the present work is to determine the best conditions to measure the fracture

toughness of ASTM A-743 grade CA-6NM stainless steel used in hydraulic turbine runners. For this purpose, fracture toughness J_{IC} tests are performed on smooth and side-grooved compact tension (CT) specimens of different thicknesses. Tests are carried out based on ASTM E1820 guide lines [11]. The investigated material and the experimental technique are first presented. Results of mechanical tests are analyzed and compared; fractographic examinations are also made in the crack growth regions in order to interpret the fracture mechanisms of the tested steel.

2. Material studied

The experimental material studied in this work is a low carbon CA-6NM steel (13Cr-4Ni martensitic stainless cast steel). Table 1 gives the chemical composition limits of the tested material as required by ASTM A-743 standard [12]. Heat treatment consisted of austenitizing at 955 ^{o}C followed by air cooling. Then, a tempering was performed between 565^{o}C and 620^{o}C allowing the fresh martensite to temper, giving rise to a beneficial softening corresponding to reduce hardness but increase ductility. The resulting microstructure is mainly tempered martensite with about up to 15% reformed austenite. The basic mechanical properties have been characterized in an early study [1]. For brevity, only tensile properties are given here. The measured yield strength σ_{YS} is 763 MPa, the tensile strength σ_{TS} is 837 MPa and the elongation is 27%. All measured mechanical properties meet ASTM A-743 standard requirements.

Table 1. Chemical composition limits of tested steel (wt.%)

	C	Mn	Si	S	P	Cr	Ni	Mo
CA-6NM	0.03	0.57	0.37	0.02	0.02	12.68	4.03	0.67
ASTM A-743	0.06 max	1.0 max	1.0 max	0.03 max	0.04 max	11.5-14.0	3.5-4.5	0.4-1.0

3. Mechanical testing

Standard compact tension (CT) specimen according to the recommendations of ASTM designation E1820 is used. The geometry of J_{IC} test specimen (Figure 1) allows the measurement of load line displacement (LLD) by means of an extensometer. One 12.7 mm thick smooth specimen without side grooves was first tested. Then five side-grooved specimens were tested: two specimens with B = 12.7 mm (*B/W =1/4)* and three specimens with B = 25.4 mm (*B/W =1/2).* Side grooves have each a depth of 10% of the gross thickness B. As the tested material is in a cast condition, there is no need to orientate it during machining. All tests were carried out at room temperature using partial unloading compliance method on a servo-hydraulic testing machine. The tests followed the guide-lines of the ASTM E1820 standard for the fracture toughness determination from a single specimen.

For the fatigue pre-cracking, two different procedures were assessed. First, four specimens were pre-cracked prior to the side-grooving operation as recommended by E1820 standard. The crack growth was followed by an optical microscope on specimen polished surfaces. Secondly, two other specimens were pre-cracked after the side-grooving operation, side grooves were machined at the same time as the specimens. In this case, the pre-cracking is monitored by a COD gage using elastic-compliance method. For all specimens, the pre-crack length is about 5 mm, providing an a_0/W value of 0.55. During pre-cracking, the loading ΔK is kept to 12 MPa$\sqrt{m}$ in order to limit the plastic zone size.

During the experiments, the specimens are subjected to about 20 loading/unloading cycles. The

unloading ratio is 10 % of actual maximum load. A representative experiment is shown in Figure 2 for a 12.7 mm thick side-grooved specimen. After the final unloading, the specimen was marked by heat tinting (450^{o}C for 1 hour). The initial and final crack lengths a_0, a_f are measured at 9 equally spaced locations on the broken specimens.

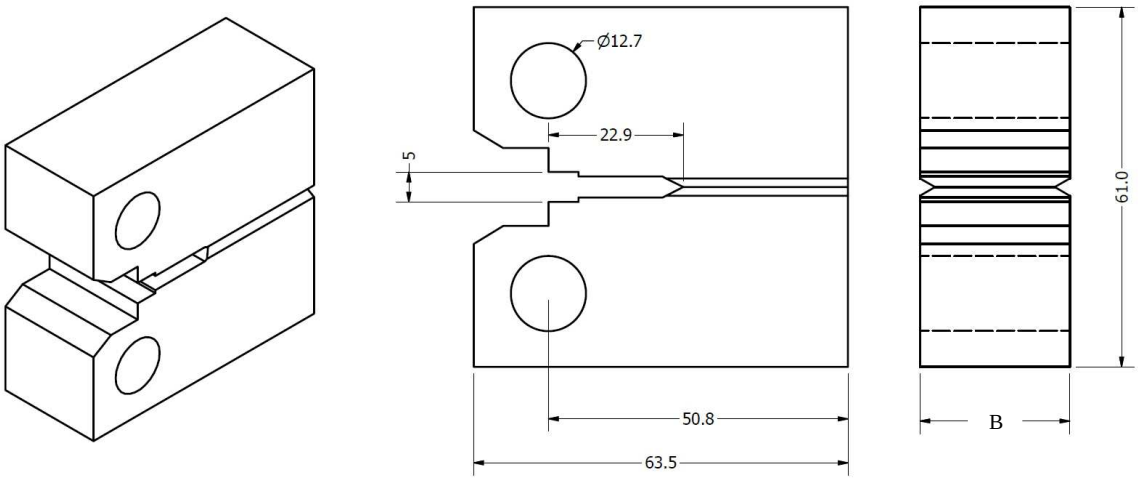

Figure 1. Compact tension J_{IC} specimen with side grooves (dimensions in mm); specimen gross thickness B is 12.7 mm or 25.4 mm; the side groove depth is $0.1B$ at each side.

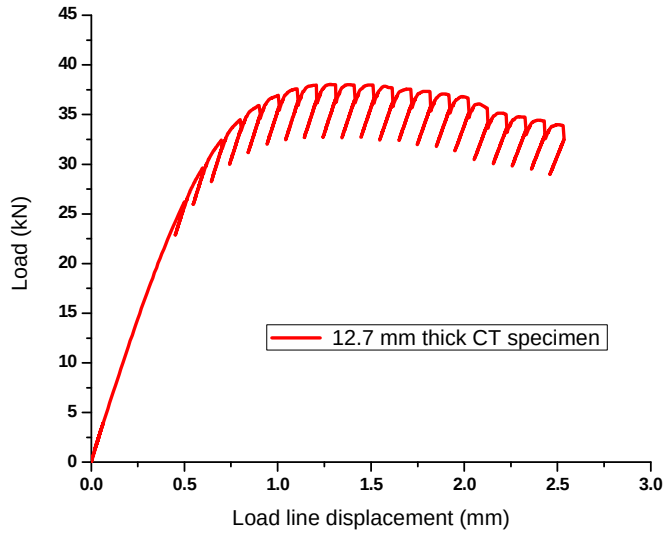

Figure 2. Load – load line displacement curve (10% unloading)

4. Results and discussion

4.1 Results

4.1.1 J_{IC} testing

Figure 3 shows a representative *J-Δa* curve obtained from the previous 12.7 mm thick side-grooved specimen. The blunting line is calculated from material tensile properties as following,

$$J = 2\sigma_Y \Delta a \tag{1}$$

$$\text{and} \quad \sigma_Y = \frac{\sigma_{YS} + \sigma_{TS}}{2}$$

The data points lie between the 0.15 mm offset line and 1.5 mm offset line parallel to the blunting line ($J = 2\sigma_Y \Delta a$) are used for regression line fitting. They can be represented by a power-law expression $J = A(\Delta a)^b$. The intersection point between the regression line and 0.2 mm offset line gives a candidate value J_Q which becomes J_{IC} provided that the validity requirements are satisfied.

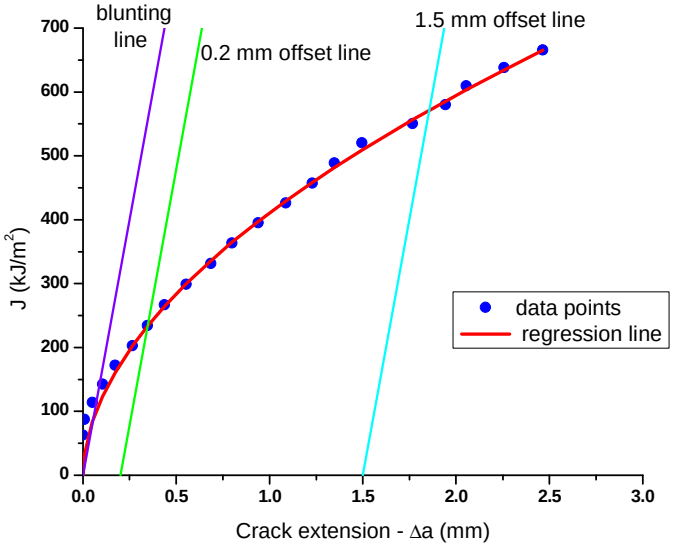

Figure 3. *J-Δa* curve for the 12.7 mm thick CT specimen

Then, K_{IC} can be estimated by

$$K_{IC} = \sqrt{\frac{EJ_Q}{(1-\nu^2)}} \tag{2}$$

where E is Young's modulus of the steel tested and ν is Poisson's ratio.

Table 2 gathers all test results on both 12.7 mm and 25.4 mm thick side-grooved specimens. For the smooth specimen (B = 12.7 mm) which was firstly assessed in the present study, no valid data point is found due to an extremely steep *J-Δa* curve. There is no intersection between the regression line and 0.2 mm offset line. So the testing result is not given here.

Table 2. Testing results of J_Q for CA-6NM steel

Specimen thickness (mm)	Test	J_Q (kJ/m^2)	dJ/da (MPa)	K_{IC} (MPa$\sqrt{m}$)
12.7	CT_05in_1	232	220	230
	CT_05in_2	280	210	252
25.4	CT_1in_1	256	128	241
	CT_1in_2	255	133	240
	CT_1in_3	286	124	255

As shown in Figure 4, there is little difference at the beginning of crack extension between 12.7 mm and 25.4 mm thick side-grooved specimens. Similar fracture initiation toughness J_Q values can be

obtained on both specimens. However, in the following crack growth region (Δa > 0.5 mm), thin specimen gives a steeper *J-Δa* curve and exhibits higher load carrying capacity than the thick sample. The tearing moduli *dJ/da*, which is more representative of crack propagation, is much higher for thin specimens than thick specimens (see Table 2).

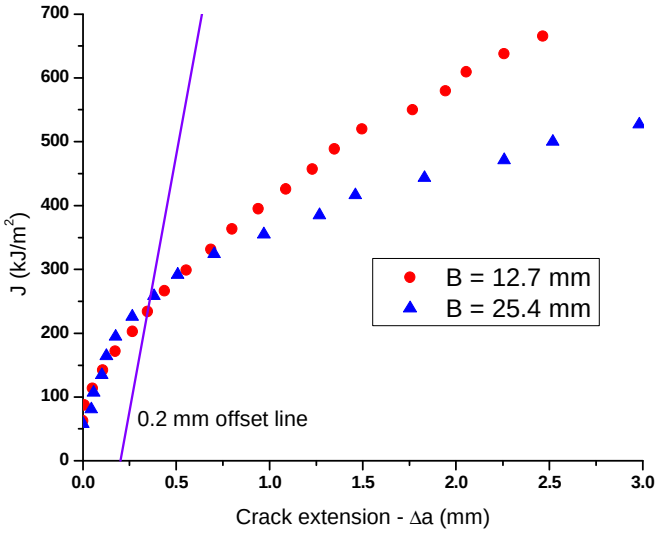

Figure 4. Effect of specimen thickness on *J-Δa* curve

4.1.2 Fractography

Fracture surfaces are firstly examined at the macroscopic scale on both 12.7 mm and 25.4 mm thick samples (see Figure 5). In the 12.7 mm thick smooth specimen (Figure 5a), strong crack tunneling is observed. There are no crack growths at both side surfaces of specimen while the crack advances more than 2 mm in the center section of the specimen. In the 12.7 mm thick side-grooved specimen (Figure 5b), crack tunneling is less pronounced, but the crack grows again faster in the center section of the specimen than near the specimen surfaces. As it is stated in section 9.1 of E1820 standard, such a test cannot be valid due to the strong crack front curvature. In the 25.4 mm thick side-grooved specimen (Figure 5c), crack grows with the same rate at the center of the specimen as at the two side surfaces. The crack extension front is nearly straight, and the test is valid according to E1820 standard. In the final ductile tearing (white part of Figure 5), we can also see that there is stronger lateral contraction in the thin specimen than in the thick one.

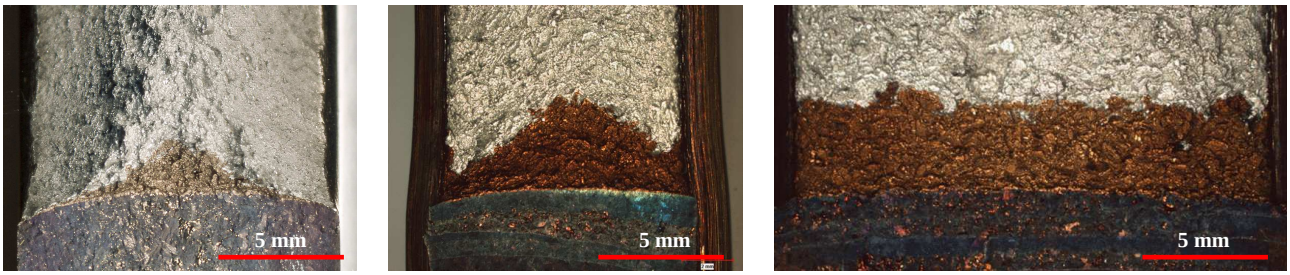

(a) (b) (c)

Figure 5. Fracture surface of broken specimens: (a) 12.7 mm thick smooth specimen, (b) 12.7 mm thick side-grooved specimen, (c) 25.4 mm thick side-grooved specimen. Crack front at the end of stable propagation was marked by heat tinting.

In order put into evidence the fracture mechanisms at microscopic scale, one 25.4 mm thick

side-grooved specimen was marked under fatigue instead of heat tinting after the final unloading. Broken sample was observed using scanning electron microscopy. In the stable crack extension region (Figure 6) void growth mechanism is dominant. Very large dimples can be seen, their size being about 20 μm. At a higher magnification (Figure 6b), the presence of inclusions in the bottom of dimples is clearly visible. It can be interpreted by the high stress triaxiality (plane-strain state) which triggers a fast void growth leading to formation of large dimples [13].

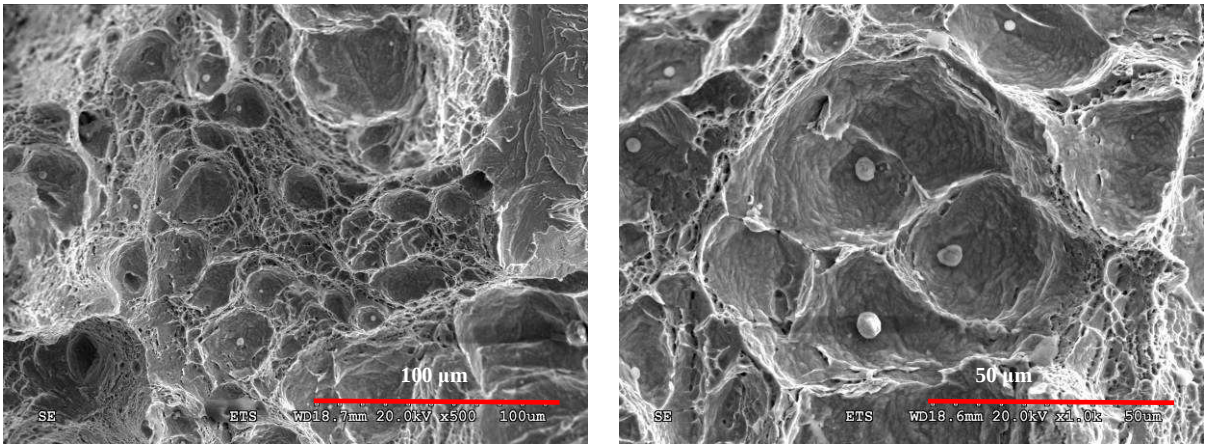

(a) (b)

Figure 6. SEM micrography of a broken specimen in the stable crack growth region

4.2 Discussion

4.2.1 Constraint effects

From the present study, experimental results show that the crack extension behavior is related to the variation of stress triaxiality across the specimen thickness. In 12.7 mm thick smooth specimen, strong crack tunneling is observed because of relatively low stress triaxiality and constraint level across the whole specimen thickness. And final fracture by ductile tearing or shearing can be seen on broken surfaces. In 12.7 mm thick side-grooved specimen, lateral constraint is increased by side grooving operations, and flat ductile fracture is observed. But the specimen is not thick enough to get a full constraint across the thickness and which caused a final curved crack front. In 25.4 mm thick side-grooved specimen, a perfectly straight crack front is obtained after stable crack extension. Because the side grooves promote practically uniform plane strain constraint along the crack front [14]. Similar results were reported in [15-18] for CT and SENB testing with various smooth and side-grooved specimen sizes.

Our investigations also show that the variation of stress triaxiality or thickness constraint leads to changes on the shape of *J-Δa* resistance curve after certain amount of crack extension. The slope of the *J-Δa* curve for the thin specimen is significantly steeper than the corresponding value for the thick specimen. In other words, thin specimen exhibits higher load carrying capacity (*dJ/da*) than thick specimen. It is known that the lateral constraint and average stress triaxiality increases with increasing specimen thickness. For thick specimen, the high stress triaxiality reduces the apparent ductility of the material by a faster void growth mechanism which is predominant as shown in Figure 6 in the previous section. While for thin specimen, the average stress triaxiality is lower and the lateral contraction is less constrained during the loading, so a relatively steeper resistance curve is generated.

4.2.2 Side-grooves and fatigue pre-cracking

Side-grooved specimen is recommended by E1820 when the compliance method of crack size prediction is used. One objective of using side-grooved specimen is to create a straight crack front to reduce the number of tests invalided by curved crack front. In this study, 0.2B side-grooved specimens were used after having an invalid test with a smooth specimen. In order to produce nearly straight fatigue pre-crack fronts, the pre-cracking is suggested to be performed prior to the side-grooving operations by E1820. However, this procedure is time consuming. The specimen needs to be polished on two surfaces in order to monitor the crack length with an optical microscope and the pre-cracked specimens have to be returned to the machine shop for side grooves machining. Moreover, the fatigue pre-cracking front is not straight. The crack grows faster in the center section of the specimen than near the specimen surfaces even with low pre-cracking load (ΔK = 12 MPa$\sqrt{m}$ in present work). As shown in Figure 7a, the crack measured on the specimen surfaces by microscopy is shorter than the real average crack length measured on the broken surface. This curvature probably results from slower crack growth under plane stress condition.

As mentioned earlier, two specimens with side grooves machined before the pre-cracking operations were also prepared. The crack growth is followed by a COD gage with the elastic compliance method. Experiments show a good agreement between calculated crack length by elastic compliance and the measured crack length on final broken specimens. With this procedure, polished surfaces are no longer needed and the side grooves are machined at the same time as the specimen itself. Time and machining cost can be saved. For the fatigue pre-cracking, due to a relative constant constraint level across the thickness, an approximately straight crack front is produced (Figure 7b).

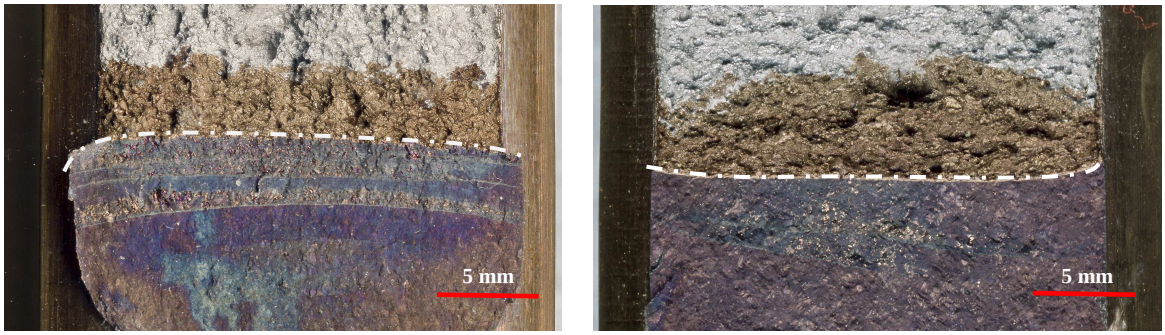

(a) (b)

Figure 7. (a) Fatigue pre-cracking performed before side grooves operation and (b) fatigue pre-cracking performed after side grooves operation. White dashed line: fatigue pre-cracking front.

5. Conclusions

J_{IC} fracture toughness testing was performed on CA-6NM martensitic stainless steel, the following conclusions are drawn:

1. Due to high toughness of the material, side-grooved specimen must be used in order to get a valid test according to ASTM E1820. Side grooves can prevent the development of crack tunneling and to maintain a relatively straight crack growth.
2. Crack growth exhibits a thumb-nail front for both 12.7 mm thick side-grooved CT specimens. It cannot be valid per ASTM standard due to the significant curvature of final crack front.

3. Valid tests are obtained with 25.4 mm thick side-grooved CT specimens with a straight crack extension front.
4. Both thin and thick specimens give very close *J* values at crack initiation (0.2 mm offset line). So, thin specimen can also be used if only crack initiation toughness is required. It is recommended that thicker specimen should be used if the plane strain *J*-resistance curve is required.
5. Side grooves can be machined before the pre-cracking; it can reduce the preparation time and machining delay and it gives a straight pre-cracking crack front. No significant difference was found on the fracture toughness testing as recommended by ASTM E1820 (pre-cracking before side grooving).
6. Fractography analysis shows that the void growth from inclusions is dominant in the crack extension region; large dimples are observed which can be explained by the high stress triaxiality of specimen.

Nomenclature

a	Crack length (mm)	b_0	Uncracked ligament length (mm)
Δa	Crack extension (mm)	σ_{YS}	Yield stress (MPa)
B	Specimen gross thickness (mm)	σ_{TS}	Ultimate tensile stress (MPa)
B_N	Specimen net thickness (mm)	E	Young's Modulus (GPa)
W	Specimen width (mm)	ν	Poisson's ratio
K	Stress intensity factor (MPa$\sqrt{m}$)	J	J-integral (kJ/m^2)
K_{IC}	Fracture toughness (MPa$\sqrt{m}$)	J_Q	Fracture toughness (kJ/m^2)

Acknowledgements

The authors thank Alstom Power Hydro, Hydro-Québec and National Research Council of Canada for financial support. The authors also wish to thank Carlo Baillargeon, Technologist at Hydro-Québec, for his experimental assistance in this study.

References

[1] J. Lanteigne, M. Sabourin, T. Bui-Quoc, D. Julien, The characteristics of the steels used in hydraulic turbine runners, 24th Symposium on hydraulic machinery and systems, Foz do Iguassu (2007).
[2] W.P. Casas, S.L. Henke, N. Novicki, Fracture toughness of CA6NM alloy, quenched and tempered, and of its welded joint without PWHT, Welding International 23 (2009), pp. 166–172.
[3] P. Blimes, C. Llorente, J. Perez Ipina, Toughness and Microstructure of 13Cr4NiMo high-strength steel welds, Journal of Materials Engineering and Performance 9(6) (2000) 609–615.
[4] M. Sabourin, B. Papillon, L. Mathieu, D. Julien, Francis runner fabrication process corner stone of power plant reliability , HydroVision, Montréal (2004).
[5] M. Sabourin, D. Bouffard, F. Paquet, Life prediction of hydraulic runner using fracture mechanics analysis, WaterPower XV, Chattanooga (2007).
[6] ASTM E399-09, Standard test method for linear-elastic plane-strain fracture toughness K_{IC} of metallic materials, American Society for Testing and Materials, 2009
[7] T.L. Anderson, Fracture Mechanics, Fundamentals and Applications, CRC Press, Taylor & Francis Group, 2005

[8] J.A. Begley, J.D. Landes, The J-integral as a fracture criterion, Fracture toughness, ASTM STP 514, American Society for Testing and Materials, 1972, pp. 1-23
[9] J.D. Landes, H. Walker, G.A. Clarke, Evaluation of estimation procedures used in J-integral testing, in: ASTM STP 668, American Society for Testing and Materials, 1979, pp. 266-287
[10] J.R. Rice, A path independent integral and the approximate analysis of strain concentration by notched and cracks, Journal of Applied Mechanics 35 (1968) 379–386.
[11] ASTM E1820-11, Standard test method for measurement of fracture toughness, American Society for Testing and Materials, 2011.
[12] ASTM A743-06, Standard specification for castings, iron-chromium, iron-chromium-nickel, corrosion resistant, for general application, American Society for Testing and Materials, 2006
[13] J.R. Rice, D.M. Tracy, On the ductile enlargement of voids in triaxial stress fields, Journal of Mechanics and Physics of Solids 17 (1969), pp. 210–217.
[14] C.F. Shih, H.G. deLorenzi, W.R. Andrews, Elastic compliance and stress-intensity factors for side-grooved compact specimens, International Journal of Fracture 13 (1977), pp. 544–548.
[15] E. Roos, U. Eisele, H. Silcher, Effect of stress state on the ductile fracture behavior of large-scale specimens, ASTM STP 1171, American Society for Testing and Materials, 1993, pp.41-63.
[16] P.S. Lam, Y. J. Chao, X.K. Zhu, R.H. Sindelar, Determination of constraint-modified J-R curves for carbon steel storage tanks, Journal of Pressure Vessel Technology 125 (2003) 136–143.
[17] X. K. Zhu, J.A. Joyce, Review of fracture toughness (G, K, J, CTOD, CTOA) testing and standardization, Engineering Fracture Mechanics 85 (2012) 1-46.
[18] B. Tanguy, T.T Luu, G. Perrin, A. Pineau, J. Besson, Plastic and damage behavior of a high strength X100 pipeline steel: Experiments and modeling, International Journal of Pressure Vessels and Piping 85 (2008) 322–335.